AGU PUBLICATIONS

Geochemistry, Geophysics, Geosystems

RESEARCH ARTICLE
10.1002/2014GC005420

Key Points:
- Modeling seismic source power levels in shallow water are difficult
- The MCS streamer can be used to estimate source power
- Power levels can vary in response to topography and geology

Correspondence to:
T. J. Crone,
crone@ldeo.columbia.edu

Citation:
Crone, T. J., M. Tolstoy, and H. Carton (2014), Estimating shallow water sound power levels and mitigation radii for the *R/V Marcus G. Langseth* using an 8 km long MCS streamer, *Geochem. Geophys. Geosyst.*, *15*, doi:10.1002/2014GC005420.

Received 14 MAY 2014
Accepted 2 SEP 2014
Accepted article online 10 SEP 2014

Estimating shallow water sound power levels and mitigation radii for the *R/V Marcus G. Langseth* using an 8 km long MCS streamer

Timothy J. Crone[1], Maya Tolstoy[2], and Helene Carton[1]

[1]Lamont-Doherty Earth Observatory, Columbia University, Palisades, New York, USA, [2]Department of Earth and Environmental Sciences, Lamont–Doherty Earth Observatory, Columbia University, Palisades, New York, USA

Abstract For seismic surveys in shallow-water environments, the complexity of local geology and seafloor topography can make it difficult to accurately predict associated sound levels and establish appropriate mitigation radii required to ensure the safety of local marine protected species. This is primarily because necessary detailed information regarding the local seafloor topography and subseafloor geology is often unavailable before a survey begins. One potential solution to this problem is to measure received levels using the ship's multichannel seismic (MCS) streamer, which could allow for the dynamic real-time determination of sound levels and mitigation radii while a survey is underway. We analyze *R/V Langseth* streamer data collected on the shelf and slope near the Washington coast during the Cascadia Open-Access Seismic Transects (COAST) and Ridge2Trench projects to measure received levels up to a distance of approximately 8 km from the sound source array. We establish methods to filter, clean, and process streamer data to accurately determine received power levels and confidently establish mitigation radii. We show that in shallow water measured power levels can fluctuate due to the influence of seafloor topographic features, but that the use of the streamer for the establishment of dynamic mitigation radii is feasible and should be further pursued. The establishment of mitigation radii based on local conditions may help to maximize the safety of marine protected species while also maximizing the ability of researchers to conduct seismic studies.

1. Introduction

An area of growing environmental concern with active source seismic experiments is the potential impact of the received sound on marine protected species, but data relating to this issue are limited. The National Marine Fisheries Services (NMFS) currently defines safety criteria (levels above which there is concern of auditory impairment or injury) for pinnipeds and cetaceans as 190 and 180 dB RMS referenced to 1 μPa, respectively. Additionally, the 160 dB level is identified as the level above which, in the view of NMFS, there is likely to be behavioral disturbance for cetaceans. The definition of these safety criteria and behavioral disturbances is controversial because they are not frequency specific, there is little data available to support them for a breadth of species, and the use of the root mean square (RMS of pressure in dB referenced to 1 μPa, which is a measure of acoustic intensity) to calculate received levels of an impulsive source leads to undesirable variability in levels and may not be most relevant in terms of animal hearing [*Madsen*, 2005]. While there are no data linking seismic sources with physical harm to marine protected species in the wild, circumstantial inferences have been made [e.g., *Gray and Waerebeek*, 2011], and some studies have shown that captive animals can experience temporary threshold shifts when exposed to seismic sources, particularly at high frequencies [e.g., *Finneran et al*., 2002; *Lucke et al*., 2009], and that caged fish have suffered hearing damage when exposed to levels in excess of 190 dB from a seismic source just 5–15 m away [*McCauley et al*., 2003]. However, mitigation methods rely in part on the ability of animals to move away from an area of sound exposure. There is evidence of such behavior [*Gordon et al*., 2004] and any such avoidance is considered a "behavioral response" which must be approved through permitting. The concern is that with critically stressed species even what seem like relatively minor changes in behavior may lead, for instance, to a reduction in foraging success and thus impact the survival of the population [*Miller et al*., 2009].

Therefore, it is important that sound level mitigation radii for seismic surveys be established for the protection of marine protected species. For the *R/V Langseth*, this is usually accomplished using direct arrival modeling and previous calibration experiments [*Tolstoy et al*., 2004, 2009; *Diebold et al*., 2010]. Propagation of

sound from seismic arrays can be accurately modeled in deep-water environments, but in shallow and sloped environments the complexity of local geology and bathymetry and the typical lack of sufficient information regarding this complexity can make it difficult to accurately predict sound levels as a function of distance from the source array. One potential solution to this problem in shallow water is to measure the received levels in real-time using the ship's streamer [*Diebold et al*., 2010], which would allow the dynamic determination of suitable mitigation radii. In this paper, we use a shallow-water survey line collected during the Cascadia Open-Access Seismic Transects (COAST) project to develop methods for establishing sound power levels using the R/V Langseth streamer in shallow water. We describe techniques for preparing the data in order to estimate RMS and sound exposure level (SEL, which is a measure of the time-integrated acoustic intensity), and estimate distances to levels of regulatory interest up to 8 km from the ship. The establishment of dynamic mitigation radii based on local conditions may help maximize the safety of marine protected species while also maximizing the ability of scientists to conduct seismic research.

2. Cascadia Open-Access Seismic Transects and Line A/T

In July of 2012, a group of scientists led by Steve Holbrook conducted a set of seismic transects on the Cascadia subduction margin during cruise MGL1212 of the R/V Langseth, also called the Cascadia Open-Access Seismic Transects (COAST) [*Holbrook et al*., 2012]. The goal of this cruise was to collect 2-D seismic reflection profiles and other geophysical data to facilitate the study of a variety of processes associated with the subduction of the Juan de Fuca plate beneath the North American plate along the Cascadia margin. The group collected seismic data along 12 transects, many of which took the ship's seismic array and streamer into the relatively shallow waters of the continental shelf near the coast of Washington state.

During this cruise, observers sighted numerous whales while surveying in shallow waters, prompting several power-downs and shut-downs while working on the shelf. However, on one of their last lines, dubbed "Abers/Trehu," or line A/T, which was an add-on line collected for the Ridge2Trench project, the group was able to complete a $\sim$64 km seaward transect in water depths ranging from about 40 to 1400 m without power-downs, shut-downs, or diversions for other vessels. Because of this continuity and the number of shots in shallow water, we selected this line to explore methods for determining shallow water power levels using the streamer. Figure 1 shows the location of line A/T in relation to the Washington coast, including intermittent shotpoints and streamer positions, and the regional bathymetry.

The full extent of line A/T included 1277 seismic shots spaced 50 m apart using the 36 gun 6600 in^3 four-string array towed at a depth of 9 m. Shots were recorded using an 8 km streamer with 636 hydrophone groups (channels) spaced 12.5 m apart and towed at a depth of 9 m. The acquisition system (Syntron SYNTRAK 960-24) sampled the hydrophone groups at 500 Hz for 16.384 s/shot. Prior to digitization, an analog Butterworth low-cut filter at 3 Hz (6 dB/octave) and a digital finite impulse linear phase high-cut filter at 206 Hz (276 dB/octave) were applied. The 24 bit recording system has a dynamic range of 99–114 dB depending on the gain which is variable. Using the gain and hydrophone sensitivity information, the system converted the signals from the streamer into units of pressure (Pa) before writing data to a file in the SEG-D format. Using DGPS on the vessel, seismic source array, and tailbuoy, along with streamer compasses and range and bearing data from transponders on the source, streamer, and tailbuoy, positions were determined for the source and each hydrophone group for each shot. Vessel position is known with submeter accuracy. The near and far group positions are known with errors of approximately 1.5 and 4 m, respectively. The average distance between the source and the near and far groups was 263.9 $\pm$ 0.2 and 8193 $\pm$ 11 m, respectively. In this paper, we analyze 790 shots starting with shot 33,300, when the streamer is first aligned upslope along the trackline after the turn, to shot 34,089, when the source array is in a water depth of approximately 200 m.

3. Methods and Results

The process of calculating power levels and estimating distances to the 160 and 180 dB levels for each seismic shot using the streamer data involves the following steps:

1. High-pass filtering the signals to remove streamer noise.
2. Adjusting the signals to account for the group length effect.

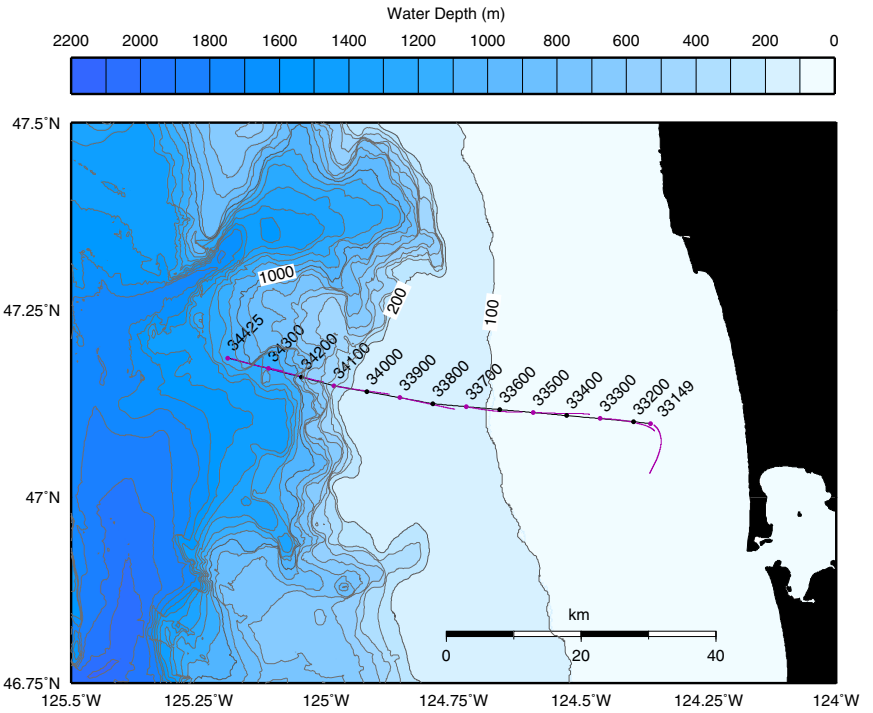

Figure 1. Contour map of the bathymetry off of the coast of Washington showing seismic line A/T studied in this paper. Shot points are labeled intermittently along the line, with those that are colored magenta also showing the position of the streamer. This line was acquired from East to West. We begin our analyses at shot 33,300 at which point the streamer is aligned upslope. See Figure 6 for a cross section of the bathymetry along the line.

3. Windowing the signals around the source impulse peak.

4. Calculating RMS and SEL for each channel on the streamer. In this paper, all RMS and SEL dB levels are referenced to the intensity and energy density, respectively, of a plane wave of pressure equal to 1 μPa [*Urick*, 1975].

5. Removing noisy or inaccurate channels.

6. Fitting an appropriate model to the data to calculate upper 95% prediction bounds for the observations and estimate four power level contours of interest, the distances to the 180 and 160 dB levels for RMS and SEL (RMS_{180}, RMS_{160}, SEL_{180}, SEL_{160}).

Because it informs our discussion of the other steps, we will first describe the process of windowing and computing RMS and SEL for impulsive signals before discussing the preceding and subsequent steps.

3.1. Windowing

For stationary (nonimpulsive) processes, calculating the RMS power of a signal is relatively straight forward. Consider a simple continuous sinusoidal pressure (p) signal as a function of time (t) given by

$$p(t) = A\sin(2\pi ft + \theta), \tag{1}$$

where A is the amplitude, f is the signal frequency, and θ is the initial phase angle with respect to the time origin. For this signal, the RMS power level over a window from t_0 to t_1 is given by [*Urick*, 1975]

$$10\log_{10}\left(\frac{1}{t_1 - t_0}\int_{t_0}^{t_1} p^2(t)dt\right). \tag{2}$$

The RMS value obtained will converge toward a single value as $(t_1 - t_0) \to \infty$. This relationship holds for a stationary random processes as well [*Bendat and Piersol*, 1986]. That is, it does not matter over what interval the RMS is calculated as long as the window is long relative to the wavelength content of the signal in question.

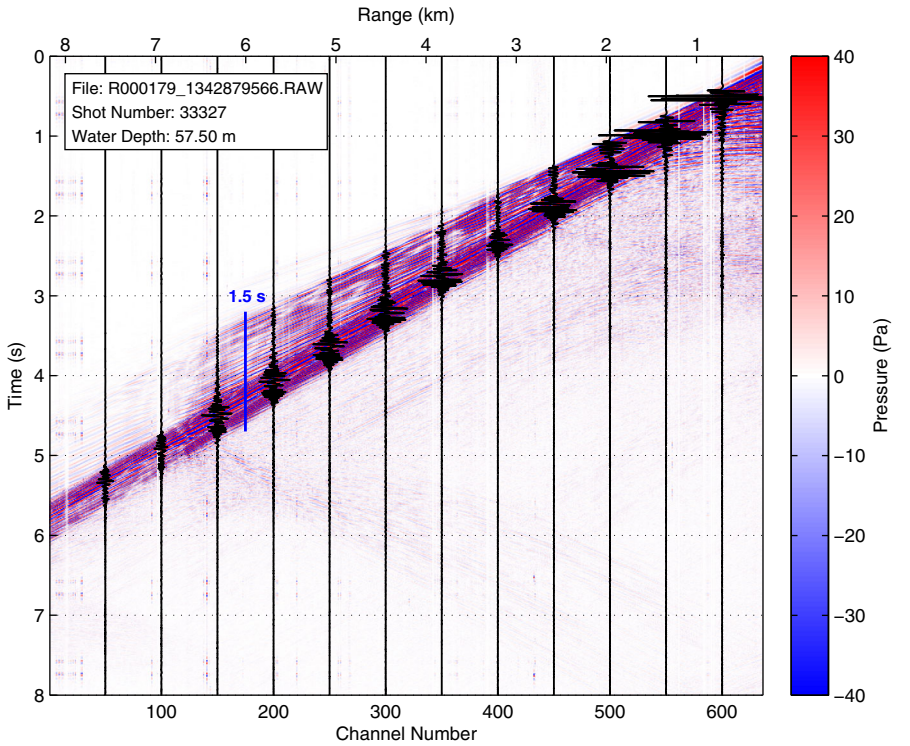

Figure 2. Colored contours of pressure for a typical shallow water shot gather overlain with a subset of waveform traces. Distance to the near group for this shot (channel 636) is 263.6 m. In shallow water, refracted arrivals from the sediment can be relatively strong and nearly coincident with direct water arrivals resulting in an impulse that can be 1.5 s or longer. Not accounting for such long impulses will result in underestimated SEL levels and overestimated RMS levels.

However, for a nonstationary random process such as the impulsive pressure signal from a seismic source array, the RMS value obtained with equation (2) can vary substantially with the choice of t_0 and t_1. As the window increases in size, the RMS tends to decrease. The solution to this problem for signals with relatively high signal-to-noise ratios has traditionally been to define a modified RMS equation given by

$$10log_{10}\left(\frac{1}{T_{90}}\int_{t_0}^{t_1} p^2(t)dt\right), \tag{3}$$

where T_{90} is defined as the length of the window that contains 90% of the total cumulative power of the signal between t_0 and t_1. This solution seems reasonable, but t_0 and t_1 still must be chosen, and it is not obvious how. According to *Madsen* [2005], this initial window should be chosen such that it includes the entire signal wave form as well as short sections of noise on either side. This directive notwithstanding, there has been little discussion of exactly how long this initial window should be for a seismic source signal, how it should be positioned relative to the wave form, and how changes in the initial window will affect the computation of RMS and SEL. In one study, *Tolstoy et al.* [2009] used an initial window that was 0.5 s long and centered on the signal peak. Other studies have used both 0.5 and 1.0 s windows [*Tolstoy et al.*, 2004; *Diebold et al.*, 2010] depending on water depth.

An examination of data from line A/T shows that because strong refracted and reflected arrivals can be coincident with the direct water arrivals in these shallow waters, the seismic source signal can be quite long. Figure 2 shows a representative shot gather from a water depth of ~60 m. Very close to the source (channels 600 and above), the signal of interest is longer because of relatively strong reflected arrivals. At more distal ranges, beyond 2 km or so, the refracted arrivals are still relatively strong and arrive just before the direct arrivals. For the shot shown in Figure 2, the amplitudes of the refracted arrivals diminish substantially beyond a distance of about 6.5 km. But for most of the gather, the received signal is greater than 1 s in length and can be as long as 1.5 s.

We explore the effect of the initial window length on RMS and also on SEL, which is equivalent to energy flux density and defined as

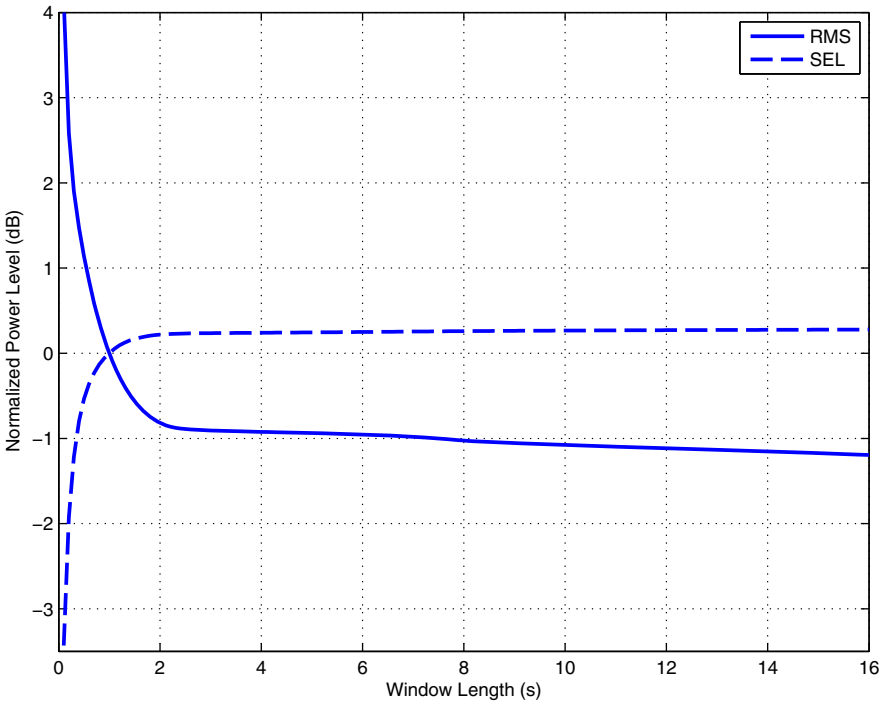

Figure 3. Normalized RMS and SEL levels as a function of window length ($t_1 - t_0$) averaged along the entire streamer and along line A/T to a depth of approximately 200 m. The RMS and SEL values have been normalized to the values computed with a window length of 1 s. For streamer data in shallow water, very little bias is introduced when including in the window large sections of noise before and after the source impulse. However, choosing a window that is too short can substantially bias power level calculations because energy from the impulse is truncated. Similarly, window position has little effect on the power levels as long as no part of the impulse is truncated.

$$10log_{10}\left(\frac{1}{T_{90}}\int_{t_0}^{t_1} p^2(t)dt\right) + 10log_{10}(T_{90}). \quad (4)$$

Figure 3 shows the average RMS and SEL levels as a function of window length averaged along the entire streamer and along line A/T to a depth of ~200 m. All values have been normalized to the values calculated using a 1 s window length so that values at different ranges can be compared. On average, window lengths that are too short tend to overestimate RMS levels because the signal is truncated which artificially decreases T_{90}. An artificially low T_{90} tends to bias SEL in the opposite direction because the second term in equation (4) is negative when T_{90} is less than unity.

For calculating RMS and SEL for impulsive signals using equations (3) and (4), it matters little how long the initial window is as long as the *entire* impulse is contained within that window. As long as the signal-to-noise ratio is high (see section 3.2 on filtering), including additional noise before and after the window does not bias the final calculation, but selecting a window that is too short will. In this study, we use an initial window that is 4 s in length and centered on the peak of each trace.

3.2. High-Pass Filtering

Because the streamer is being towed through the water at some depth below the surface, a considerable amount of low-frequency noise is generated by ocean surface waves and the motion of the streamer. To accurately calculate power levels with streamer data, this low-frequency noise must be removed with a high-pass filter. The filter should be designed to maximize the removal of streamer noise while minimizing the removal of any signal energy associated with the source impulse. To explore the effects of different filter designs on calculated power levels, we develop a series of high-pass Butterworth filters with roll-off frequencies ranging from 1 to 30 Hz. We use second-order, direct form II, three-section filters [*Orfanidis*, 1996], with stopband frequencies equaling half their corresponding passband frequencies, and 30 dB attenuation in the stopband. Figure 4 shows the normalized effect of these filters averaged along the entire streamer, along line A/T, to a depth of approximately 200 m. The average RMS level increases with increasing roll-off

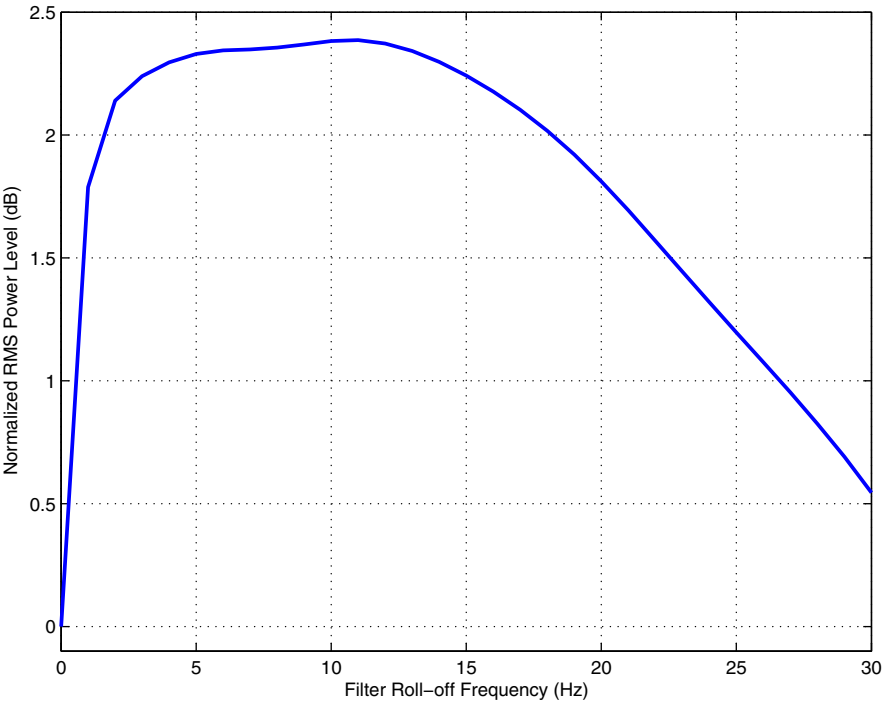

Figure 4. Normalized RMS power level as a function of high-pass filter roll-off frequency averaged along the entire streamer and along line A/T to a depth of approximately 200 m. The values have been normalized to the values calculated when the signals are not filtered, shown here with a roll-off frequency of 0 Hz. On average, maximal RMS levels are achieved when the signals are filtered at 11 Hz.

frequency until about 11 Hz, at which point the average level begins to decrease as the roll-off frequency approaches 30 Hz. The RMS level increases as the roll-off frequency approaches 11 Hz because decreasing streamer noise is included in the signal, which has the effect of decreasing T_{90}. The RMS level decreases beyond 11 Hz because signal power associated with the source impulse is being removed. In this paper, we use a filter with a roll-off frequency of 11 Hz to remove streamer noise.

3.3. Adjusting for the Group Length Effect

A single acoustic record from the streamer is not recorded by a single hydrophone, but by a set of hydrophones distributed along a short distance of the streamer. The R/V Langseth streamer has eight hydrophones spaced along every 12.5 m segment of the streamer, the signals of which are averaged to produce a single record for each shot. With such a configuration incoming horizontal acoustic energy is deemphasized because some of the energy reaching the hydrophones in a group are out-of-phase. The signals of interest for most seismic studies, incoming vertical energy from subseafloor reflections and refractions, is not attenuated. In this study, we are primarily interested in the water arrival of the source pulse which is traveling in a predominantly horizontal direction, thus we need to account for this "group length" effect. Based on both direct measurements and water column arrival modeling, *Diebold et al*. [2010] showed that the R/V Langseth hydrophone group length resulted in a 6 dB decrease in horizontal signal power levels. Their results were ground truthed with calibration buoy data. In this study, we also add 6 dB to each trace to account for this effect. Our methods including this adjustment produce essentially identical results when applied to the Diebold et al. data.

3.4. Outlier Removal

Some of the R/V Langseth hydrophone groups were not functioning correctly during the COAST survey, and recorded inaccurate levels or had excessive noise. These channels had to be identified so their data could be discarded. To determine which channels were malfunctioning, we calculated the RMS power level for every shot along line A/T and averaged the values from each hydrophone group along the line. We also calculated the RMS of channel-to-channel differentials along the streamer, averaged along the line. The first calculation gives an indication of which channels were inaccurate, and the second gives an indication of

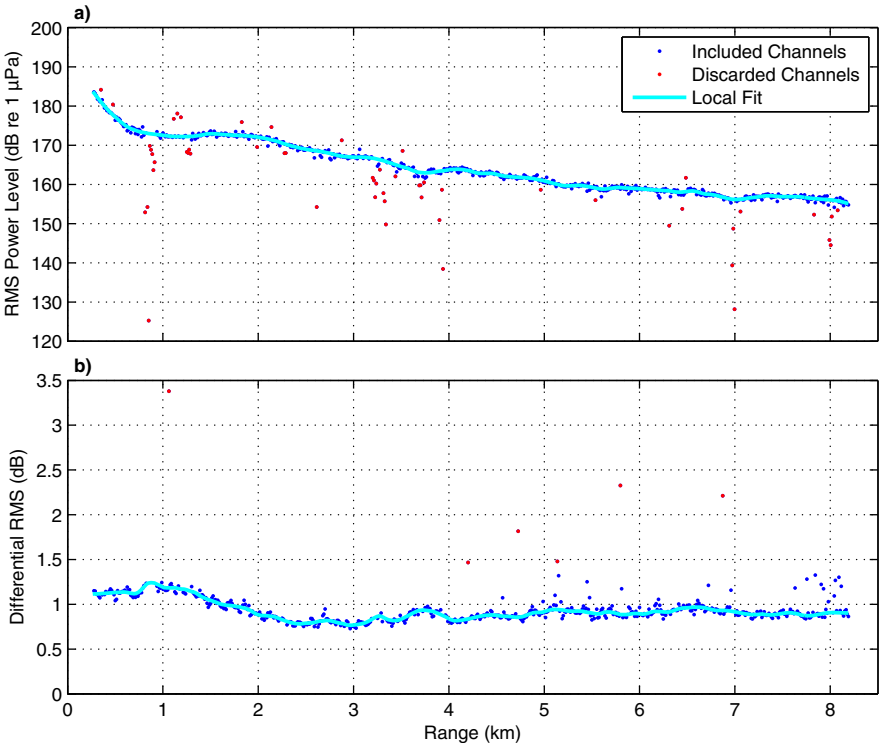

Figure 5. (a) Mean RMS power levels along the streamer, averaged along line A/T to a depth of approximately 200 m, and (b) RMS of channel-to-channel differentials. In both plots, the data have been fit using robust locally weighted regression [*Cleveland*, 1979] with a first degree polynomial model and a 20 point window. We discard channels that are 2 dB or more away from the smoothed fit to the absolute power levels and channels that are 0.5 dB or more away from the smoothed differential levels.

which were imprecise. Figure 5 shows the results of these calculations. We expect values in these scatter plots to vary smoothly along the streamer (i.e., clustered tightly along a best-fit line) because adjacent hydrophone groups that were functioning correctly should record similar average values and should not vary greatly from shot to shot. We use robust locally weighted regression [*Cleveland*, 1979] to define a best-fit to these data, and discard data from channels that have an average RMS that is more than 2 dB above or below the fitted line, and that have differential RMS levels that are 0.5 dB above or below the fitted line. In this study, we discard the data from 65 of the streamer's 636 hydrophone groups (Table 1). Most of the discarded inaccurate channels recorded levels that were below what was expected.

3.5. RMS and SEL

With the data properly prepared, we next compute the RMS and SEL values for every good channel along the analyzed section of line A/T. Figures 6 and 7 show colored contours of RMS and SEL as a function of range along line A/T, respectively, and along-track water depths. Generally, levels decrease with increasing range and increasing water depth. As the source moves beyond the shelf break, at approximately shot 34,089, data from the streamer becomes highly variable and not reliable for the determination of absolute power levels. The small bathymetric feature at approximately shot 33,450 appears to affect received levels by shadowing the streamer starting at shot 33,500. Once the entire streamer is past this feature, by about shot 33,650, shadowing stops.

Table 1. Omitted Channels

Inaccurate channels	10, 15, 16, 17, 30, 92, 97, 98, 99, 138, 141, 152 214, 260, 342, 343, 345, 349, 358, 360, 361, 362 376, 382, 390, 391, 392, 395, 398, 399, 400, 401 427, 448, 474, 475, 486, 498, 511, 554, 555, 556 557, 561, 562, 565, 568, 583, 584, 585, 586, 587 588, 589, 590, 592, 619, 629, 636
Imprecise channels	107, 193, 246, 279, 321, 572

The area of elevated RMS levels in Figure 6, in a band running from the beginning of the line to the shelf break in the range ~0 to 3 km, is caused primarily by the sensitivity of RMS to the length of the received signals. In this band, the signals (i.e., values of T_{90}) are short because the strength of reflections are diminished and the refracted

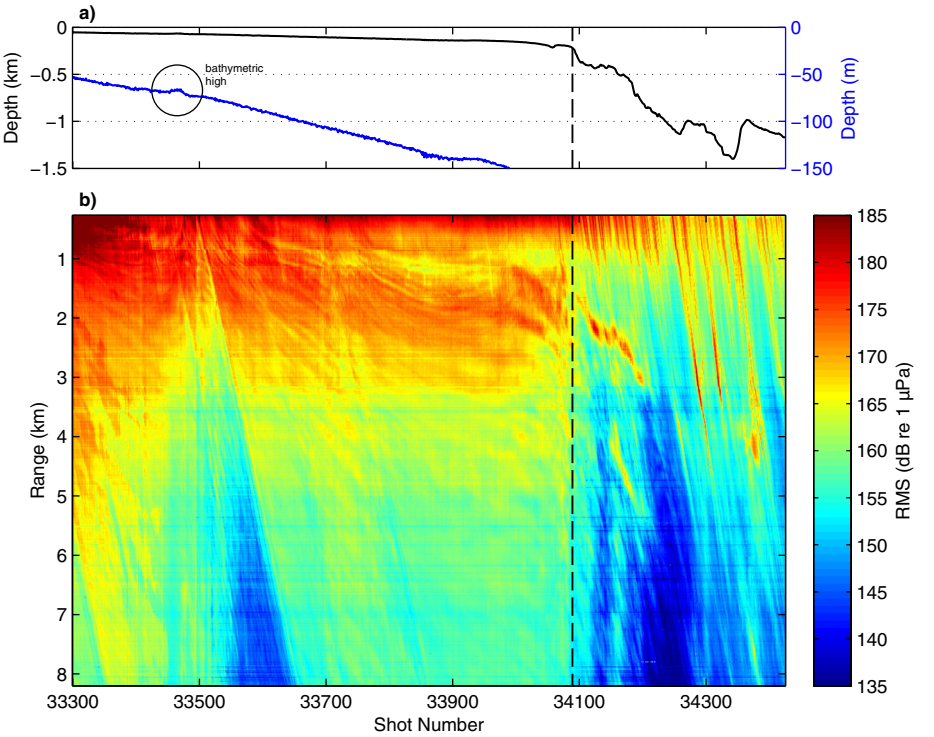

Figure 6. (a) The seafloor depth profile along line A/T and (b) colored contours of the RMS power level as a function of source to receiver distance (range) and shot number. The depth profile is plotted on two different vertical scales (with the blue profile plotted against the right-hand scale) so that in the shallow part of the line the small bathymetric high can be seen. This small ~4 m high and ~1200 m long feature shadows acoustic energy received by the streamer from about shot 33,500 to 33,650. The dashed line indicates the approximate position of the shelf break at a depth of ~200 m, at which depth for this line power level estimates become unreliable.

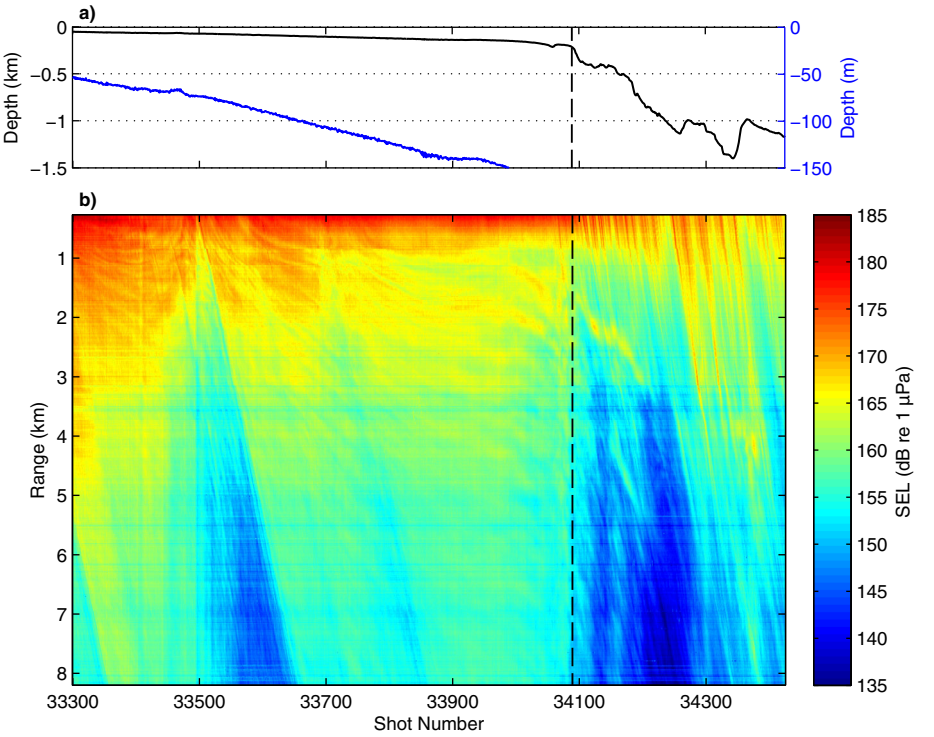

Figure 7. Values of SEL values plotted with colored contours as in Figure 6.

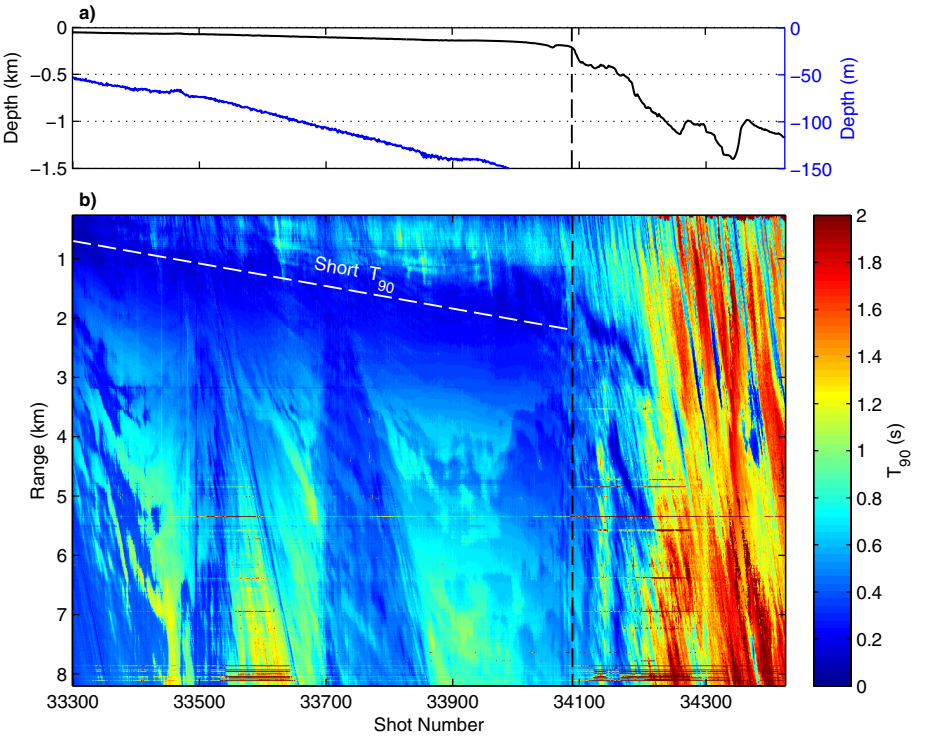

Figure 8. Values of T_{90} plotted with colored contours as in Figure 6.

energy has not moved out from the direct arrival, so RMS is elevated in this band, whereas SEL is not. Figure 8 shows the contours of T_{90} as a function of range along line A/T, similar to how they are shown in Figures 6 and 7. The band where received signals are short is highlighted with the white dashed line. Signals received by the streamer become longer beyond the shelf break primarily because the impulse at the surface is lower in amplitude so energy is spread out over a longer period of time.

Figure 9 shows the contours of the difference between RMS and SEL as a function of range along line A/T, similar to how they are shown in Figures 6 and 7. Only for a very few shots, mostly at the beginning of the line and at short ranges, is the difference between RMS and SEL 10 dB or more. Although for permitting purposes it is often assumed that RMS is 10 dB greater than SEL [*Greene*, 1997], this requires that T_{90} be 0.1 s or smaller (see equation (4)). Along line A/T, T_{90} is almost always longer than 0.1 s, and is sometimes longer than 1 s, meaning that even before the shelf break SEL is sometimes larger than RMS. On average, along this line before the shelf break RMS is 3.35 dB greater than SEL, corresponding to an average T_{90} of 0.51 s.

3.6. Models and Prediction Bounds

In order to estimate distances to the 180 and 160 dB contours for each shot, it is necessary to fit a model to the data which will allow for the estimation of the 95% prediction bounds as well as for extrapolation to distances beyond the ends of the streamer wherever necessary and prudent. We found that different models performed better for the determination of different radii. Figures 10 and 11 show example shots from line A/T along with model fits and prediction bounds used to estimate power level radii.

3.6.1. Spline Model

For almost every shot along line A/T, the streamer directly measures 180 and 160 dB levels for RMS and SEL, respectively, meaning that extrapolation is not necessary to estimate the RMS_{180} and SEL_{160} contours. For these distances, the best model is a nonparametric smoothing cubic spline model which does not make assumptions about the underlying physics. Such a nonparametric model is preferred because the underlying physics in shallow water can be complicated, as it can be strongly influenced by bottom type and topography, subseafloor structure, and water column properties. A spline model can follow the data well without having knowledge of these influences a priori. Our cubic spline model minimizes

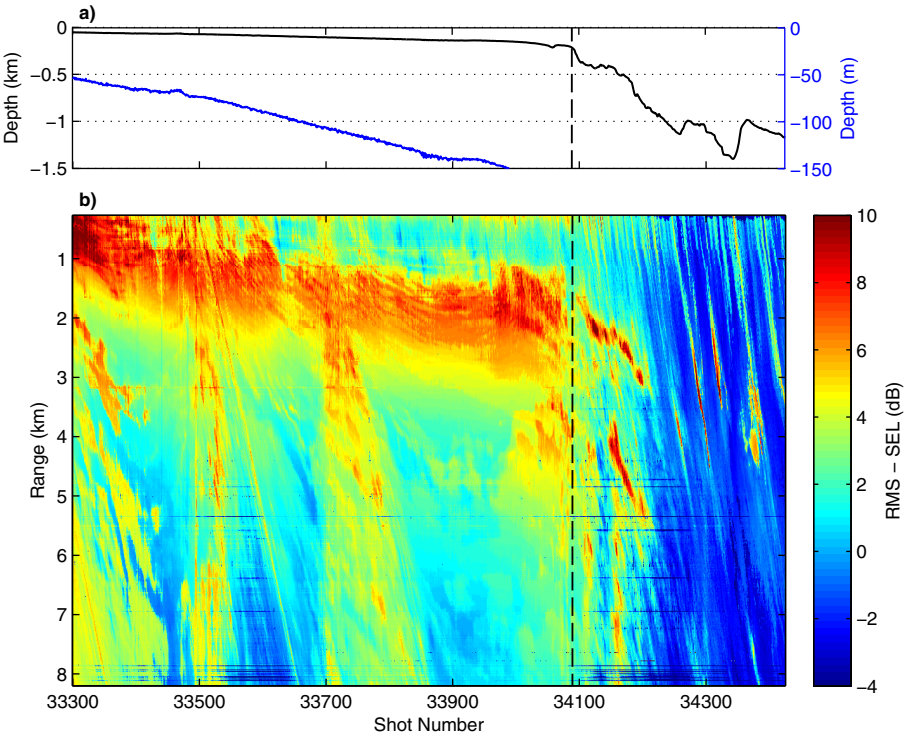

Figure 9. Values of the difference between RMS and SEL plotted with colored contours as in Figure 6.

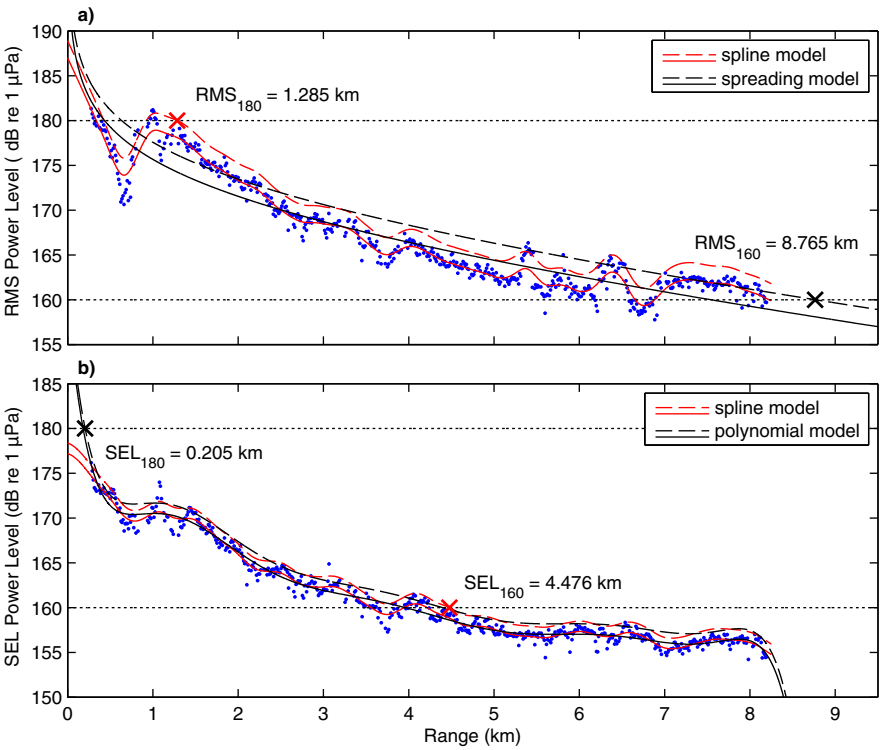

Figure 10. Example shots showing estimated (a) RMS and (b) SEL levels along with the models used to establish the 180 and 160 dB radii. The solid lines are model fits, and the dashed lines are the approximate 95% upper prediction bounds. For RMS, we use the spline and the spreading model to estimate the 180 and 160 dB radii, respectively. For SEL, we use the high-order polynomial and the spline model to estimate the 180 and 160 dB radii, respectively. The red and black "X" markers show the locations of the intersection of the upper prediction bounds used with the 180 and 160 dB radii indicated with dotted lines.

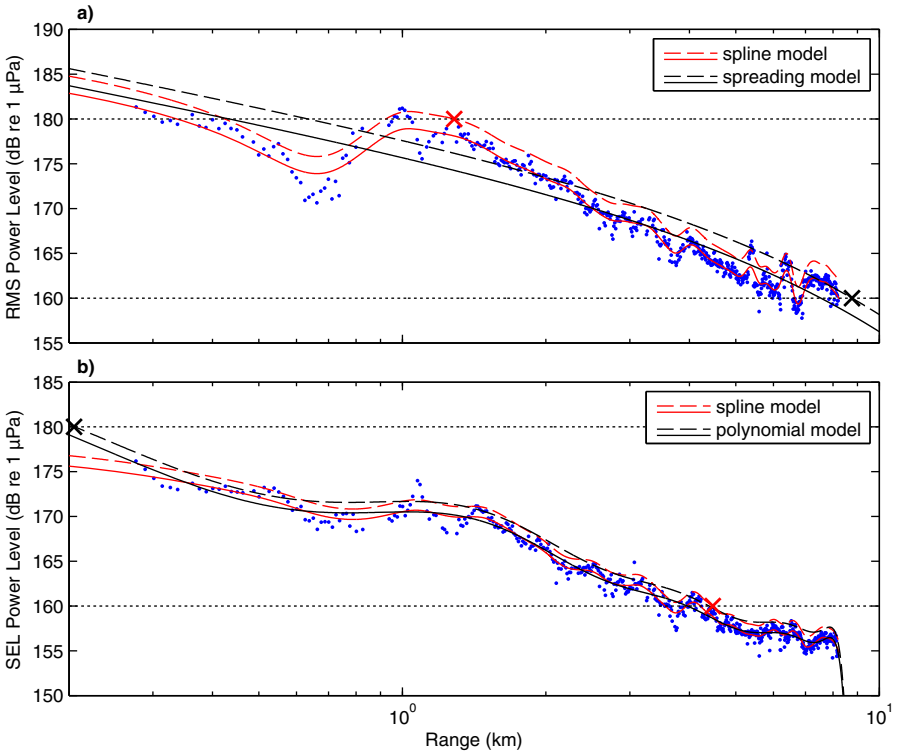

Figure 11. The same data and model fits as in Figure 10, with the range shown on a logarithmic scale.

$$p\sum_i (y_i - s(x_i))^2 = (1-p)\int \left(\frac{d^2 s}{dx^2}\right)^2 dx, \tag{5}$$

where s is a piecewise cubic spline, y_i are measurements of power level, x_i are ranges, and p is a smoothing parameter. We found empirically that a smoothing parameter of 0.9995 works best for the streamer data collected along this line. We use the 95% confidence interval derived from the residuals of this fit to establish the upper 95% prediction bound. This model and the prediction bounds are shown with red solid and dashed lines, respectively, in Figures 10 and 11. The red "X" markers show the positions of the RMS_{180} and SEL_{160} estimates for these shots.

3.6.2. Spherical Spreading Model

The RMS_{160} contour is sometimes near or just beyond the end of the R/V Langseth streamer. For this reason, extrapolation can be necessary, requiring that we use a parametric model which is better behaved beyond the data compared to the nonparametric model. We found that the best model for determining the RMS_{160} distance is a spherical spreading model with a attenuation term taking the following form:

$$y = a_1 + a_2 log_{10}(x) + a_3 x. \tag{6}$$

A linear least squares method is used to fit this model to the data. The upper prediction bound is taken from the spline model fit because in many cases large excursions from the model well away from the area of interest unduly influence the prediction bounds for this model. We allow extrapolation to a distance that is approximately 133% of the length of the streamer, or 11 km. An example of this model and the upper prediction bound is shown with black and dashed lines, respectively, in Figures 10 and 11 (top plots). The black "X" marker in these bottom plots show the position of the RMS_{160} estimate.

3.6.3. Polynomial Model

The SEL_{180} contour is often closer to the ship than the near group, requiring that we extrapolate a short distance, usually less than 100 m, to estimate the distance to the SEL_{180} contour. We found that the best model for extrapolating this short distance is a high-degree polynomial, taking the following form:

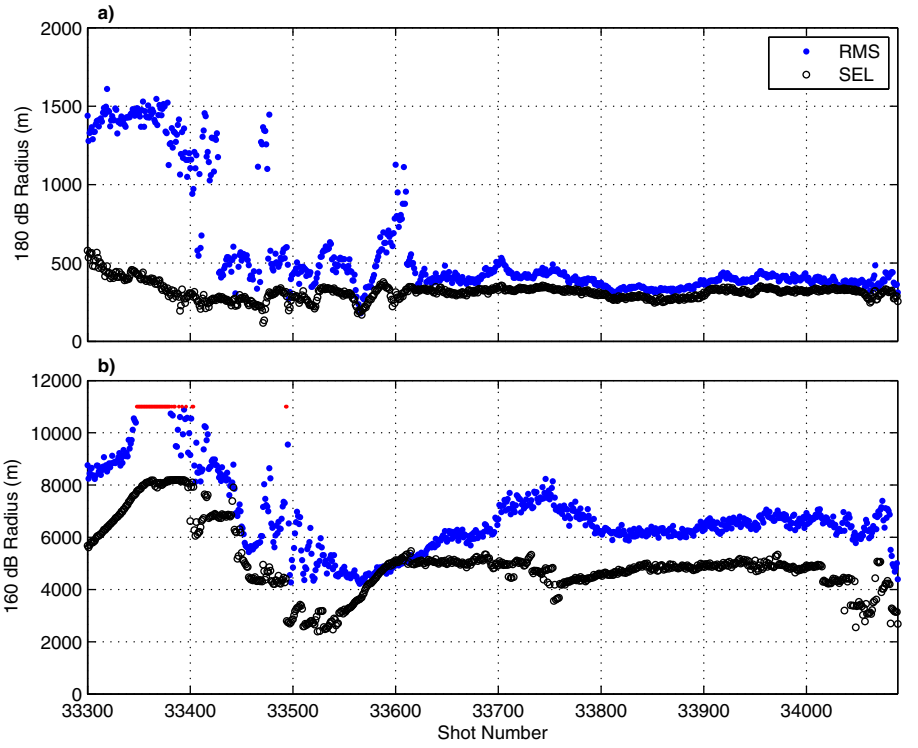

Figure 12. Estimated distances to the (a) 180 and (b) 160 dB radii along line A/T. We only estimate the 160 dB RMS radius to a distance of ~133% the length of the streamer, or 11 km. The red dots indicate where the estimate would fall outside this range.

$$y=\sum_{i=1}^{n+1} a_i x^{n+1-i}, \tag{7}$$

where $n = 9$. We calculate the 95% observation prediction bounds [*Kutner*, 2005] and use the intersection of the upper bound with the 180 dB level to estimate SEL_{180}. This model has sufficient freedom to fit these data well, but is also relatively well behaved when extrapolating short distances. An example of this model and the upper prediction bound is shown with black and dashed lines, respectively, in Figures 10 and 11 (top plots). The black "X" marker in these bottom plots show the position of the SEL_{180} estimate.

3.7. Estimated Radii

Figure 12 shows the estimated 180 and 160 dB radii for both RMS and SEL along line A/T. In general, all four contours of interest decrease with increasing water depth. In shallow water, between shots 33,300 and ~33,450, RMS_{180} is elevated primarily because the signal length and thus T_{90} are especially short for these shots at ranges between 1 and 2 km. The associated increase in RMS (see Figure 10) at these distances can extend the estimate of RMS_{180} to similar distances. The effects of signal length associated with incoming reflected and refracted arrivals are less pronounced for SEL so this does not occur for SEL_{180}. For similar reasons, RMS_{160} is elevated in the shallowest part of this line and also in the vicinity of shot 33,750. The sinusoidal shape of SEL_{160} between shots 33,300 and 33,600 results in part because of the bathymetric feature which focuses and then defocuses, or shadows, seismic energy along this section of the line.

4. Discussion

4.1. RMS Versus SEL

In his paper, *Madsen* [2005] makes a compelling argument against the use of RMS (equation (3)) for the determination of safe exposure levels and mitigation radii for marine protected species, partially on the grounds that this measure does not take into account the total acoustic energy that an animal's auditory system would experience. *Madsen* [2005] recommended the use of SEL as well as measures of peak pressure

Table 2. Predicted RMS Mitigation Radii Used During the COAST Survey and Radii Measured in This Study

	Predicted (m)		Measured (m)	
Water Depth (m)	RMS_{180}	RMS_{160}	RMS_{180}	RMS_{160}
<100	2,140	20,550	179–1,610	4,220–unconst.
100–1,000[a]	1,540	12,200	304–532	4,391–8,233
>1,000	940	3,850		

[a]Measured only to a depth of 200 m.

to establish impulsive source thresholds used for mitigation. *Southall et al*. [2007] came to similar conclusions.

Our work should provide further motivation for a regulatory move away from RMS power levels for marine protected species mitigation purposes. In shallow waters especially, interactions between direct, reflected, and refracted arrivals of acoustic energy from the array can result in large variations in signal length (T_{90}), and commensurate large variations in RMS without necessarily significant changes in exposure level. The use of SEL, which accounts for signal length, should be preferred for mitigation purposes in shallow water.

4.2. Water Depths

Mitigation radii can only be reliably established with the streamer in shallow water, perhaps in depths no greater than about 200 m. In deep water, peak sound power levels are a function of depth, with peak power levels measured at increasing depths with increasing range [*Diebold et al*., 2010]. However, in shallow water where radiation patterns typically include overlapping internal reflections, refractions, and direct arrivals, there is little to no systematic dependence of power level with depth. Additional investigations into the use of the streamer for the determination of sound power levels using extant data from other surveys and perhaps new targeted calibration experiments could help refine our understanding of the effects of water depth and seafloor slope on power levels measured with the streamer in intermediate depth waters and help us to provide more concrete guidelines on the depth ranges for which the streamer can be reliably used for sound power level estimates.

4.3. Measured Versus Predicted Radii

For depths to which this method is valid, the measured radii along line A/T are consistently lower than the predicted values used to establish mitigation radii for the COAST survey. For this survey, three mitigation radii were established for the 9 m tow depth used for line A/T (Table 2). The predicted radii were roughly 2–3 times larger than the radii measured in this study. This is possibly the result of highly conservative assumptions built into the predicted radii and/or differences in bottom and subbottom properties between this site and the Gulf of Mexico site used for calibrating the predictions [*Tolstoy et al*., 2009; *Diebold et al*., 2010]. Conservative mitigation radii are preferred to those that are underestimated; however, excessively conservative radii can result the overcounting of takes, and may cause unnecessary power-downs and shutdowns like those that plagued the COAST project, and lead to large unnecessary losses of survey data.

4.4. Radiation Patterns

One potential drawback to using the streamer to measure sound power levels is that it can only provide information on acoustic radiation patterns in one direction, usually only directly behind the vessel. Previous studies have shown that power levels can vary as a function of azimuth [*Tolstoy et al*., 2009; *Diebold et al*., 2010], with across-line power levels sometimes higher than along-line levels depending on array configuration and water depth. Power levels can also vary as a function of the seafloor slope [*Diebold et al*., 2010], with power levels measured in the upslope direction often higher because of focusing, but sometimes lower because of reflections. An example of the latter effect can be seen in Figures 6 and 7 as the array is towed beyond the shelf break at shot ~34,100. Relatively small bathymetric features can also serve to focus and defocus acoustic energy and affect measured power levels along the streamer as occurred just before shot 33,500 along line A/T (Figures 6 and 7).

Diebold et al. [2010] showed that for a two-string array in deep water—conditions under which radiation asymmetry should be high—sound power level distances may be about 25% larger in the across-line direction compared to the along-line direction. Although such asymmetry is expected to be lower for a four-string array in shallow water to be conservative we recommend adding 25% to streamer estimated mitigation radii to account for any potential azimuthal variations associated with the source configuration. To

account for bottom type and slope related effects, we recommend averaging streamer estimated radii over large sections of any one line to smooth out such effects.

4.5. Streamer Sample Rates

An additional potential concern in regard to using the streamer to estimate signal power levels is the streamer sampling rate. The system currently used by the R/V Langseth can sample at rates up to 2 kHz, although for line A/T the system was only sampling at 500 Hz, providing a bandwidth of 3–206 Hz for signal power estimation. Many species of marine mammals, on the other hand, can have auditory bandwidths that extend to well above 100 kHz [*Southall et al*., 2007]. The key to resolving this apparent dilemma is to recognize that seismic source arrays like those used by the R/V Langseth generate acoustic signals with the vast majority of energy contained within frequencies below 200 Hz [*Tolstoy et al*., 2009]. Prior estimates of source array power levels using both the *Langseth* streamer and a high-bandwidth buoy-based system recording at 50 kHz showed negligible differences, emphasizing that there is greatly reduced energy at frequencies outside the streamer's detection range [*Diebold et al*., 2010].

4.6. Developing a Real-Time System

An ultimate goal of this work is to develop a real-time or near-real-time system for estimating seismic array power levels during or just prior to a survey. Primary challenges for the development of such a system include automating several steps in the process, including (1) the identification of noisy or inaccurate channels, (2) the determination of the appropriate fitting model and whether extrapolation is prudent, and (3) smoothing out shot to shot variability. Automating the identification of bad channels would likely be straightforward, and a system could probably determine which channels to discard after having only a few shots. Bad channels are sometimes also known prior to the start of a survey. Automating the fit modeling and smoothing will likely be more difficult, but with additional research into best practices using extant data, it should be possible to develop reliable algorithms. Alternative approaches include the incorporation of some user input to validate system decisions on the fly, and/or conducting short presurvey runs to assess the acoustical environment in the shallow parts of a survey area. The later approach could help mitigate the potential problems associated with radiation patterns discussed above.

4.7. Future Regulatory Frameworks

A the time of this writing, the National Oceanic and Atmospheric Administration is currently developing new guidelines for assessing the effects of anthropogenic sound on marine mammals (http://www.nmfs.noaa.gov/pr/acoustics/guidelines.htm). The new guidelines, which are still being finalized, are likely to include acoustic impact threshold levels based on SEL as well as on peak-to-peak received pressure levels, rather than RMS pressure levels. The guidelines will also likely include different effective threshold levels for different sets of marine mammals grouped in terms of their hearing capabilities, called "functional hearing groups." Although this paper has focused on using the R/V Langseth streamer to measure sound levels and mitigation radii as set forth under the current regulatory framework, the methods described could be adapted to the new framework as currently proposed. We have shown that the streamer can be used to estimate SEL and it could similarly be used to measure peak-to-peak levels. Further, as discussed above, because of the frequency content of the MCS source, the streamer could still be employed to estimate threshold levels and mitigation radii under a regime including frequency-dependent auditory weighting functions.

5. Conclusions and Future Work

1. With proper filtering and data preparation, the R/V Langseth streamer can be used to estimate the sound power levels and actual distances to the 160 and 180 dB RMS and SEL levels.

2. Typically, as long as streamer data are high-pass filtered to remove noise, the initial window used to establish T_{90} will not significantly affect the calculation of sound power levels unless the signal of interest is truncated. Long initial windows are recommended.

3. To model received levels for prediction purposes, a nonparametric model such as a piecewise cubic spline is preferred when extrapolation is not required, as in this study for RMS_{180} and SEL_{160}.

4. To model received levels to predict sound power levels beyond the end of the streamer, as was required in this study for RMS_{160}, a spherical spreading model is preferred.

5. To model received levels to predict sound power levels at ranges that are shorter than the distance to the near group, as was required in this study for SEL_{180}, a high-degree polynomial model is recommended.

6. Because signal length can vary greatly in shallow water, and RMS does not accurately reflect exposure levels, RMS is not recommended for the determination of mitigation radii.

7. The streamer can only be used to reliably determine sound power levels in shallow water, perhaps to depths no greater than approximately 200 m. Further research using extant data could be used to more precisely determine appropriate depth ranges for this method.

8. Automated real-time systems for estimating safety radii are feasible and the development of such systems should be pursued.

9. This method could be adapted for use in compliance with proposed NOAA guidelines for determining acoustic impact thresholds.

Acknowledgments

We would like to thank the late John Diebold for his early work on the development of processing algorithms for seismic streamer data which helped make this paper possible. We also thank Steve Holbrook and all co-PI's and participants of the COAST project for collecting the data used in this paper, Suzanne Carbotte for making the data from line A/T available for this study and three anonymous reviewers for thorough reviews of our manuscript. The data used in this study are available for download from http://www.marine-geo.org/tools/search/entry.php?id=MGL1212. Support for this research was provided by the Lamont-Doherty Earth Observatory and Pacific Gas and Electric.

References

Bendat, J. S., and A. G. Piersol (1986), *Random Data: Analysis and Measurement Procedures*, John Wiley, N. Y.

Cleveland, W. S. (1979), Robust locally weighted regression and smoothing scatterplots, *J. Am. Stat. Assoc.*, *74*(368), 829–836.

Diebold, J. D., M. Tolstoy, L. Doermann, S. L. Nooner, S. C. Webb, and T. J. Crone (2010), R/V *Marcus G. Langseth* seismic source: Modeling and calibration, *Geochem. Geophys. Geosyst.*, *11*, Q12012, doi:10.1029/2010GC003216.

Finneran, J. J., C. E. Schlundt, R. Dear, D. A. Carder, and S. H. Ridgeway (2002), Temporary shift in masked hearing thresholds in odontocetes after exposure to single underwater impulses from a seismic watergun, *J. Acoust. Soc. Am.*, *111*, 2929–2940.

Gordon, J., D. Gillespie, J. Potter, A. Frantzis, A. P. Simmonds, R. Swift, and D. Thompson (2004), A review of the effects of seismic surveys on marine mammals, *J. Mar. Technol. Soc.*, *37*, 16–34.

Gray, H., and K. V. Waerebeek (2011), Postural instability and akinesia in a pantropical spotted dolphin, *stenella attenuata*, in proximity to operating airguns of a geophysical seismic vessel, *J. Nat. Conserv.*, *19*, 363–367.

Greene, C. R., Jr. (1997), Physical acoustics measurements, in *Northstar Marine Mammal Monitoring Program, 1996: Marine Mammal and Acoustical Monitoring of a Seismic Program in the Alaskan Beaufort Sea, LGL Rep. 2121-2*, pp. 3-1 to 3–63, LGL Ltd., King City, Ont., and Greeneridge Sciences Inc., Santa Barbara, Calif., for BP Explor. (Alaska) Inc., Anchorage, Akad., and Nat. Mar. Fish. Serv., Anchorage, Akad., and Silver Spring, Md.

Holbrook, W. S., G. M. Kent, K. Keranen, A. Trehu, and P. Johnson (2012), Coast: Cascadia open-access seismic transects, cruise report. [Available at: http://steveholbrook.com/research/cascadia2d/COAST.html.]

Kutner, M. H. (2005), *Applied Linear Statistical Models*, McGraw-Hill, Boston, Mass.

Lucke, K., U. Siebert, P. Lepper, and M. Anne Blanchet (2009), Temporary shift in masked hearing thresholds in a harbor porpoise (Phocoena phocoena) after exposure to seismic airgun stimuli, *J. Acoust. Soc. Am.*, *125*, 4060–4070.

Madsen, P. T. (2005), Marine mammals and noise: Problems with root mean square sound pressure levels for transients, *J. Acoust. Soc. Am.*, *116*(6), 3952–3957, doi:10.1121/1.1921508.

McCauley, R. D., J. Fewtrell, and A. N. Popper (2003), High intensity anthropogenic sound damages fish ears, *J. Acoust. Soc. Am.*, *113*, 638–642.

Miller, P. J. O., M. P. Johnson, P. T. Madsen, N. Biassoni, M. Quero, and P. L. Tyack (2009), Using at-sea experiments to study the effects of airguns on the foraging behavior of sperm whales in the Gulf of Mexico, *Deep Sea Res., Part I*, *56*(7), 1168–1181, doi:10.1016/j.dsr.2009.02.008.

Orfanidis, S. J. (1996), *Introduction to Signal Processing*, Prentice Hall, Englewood Cliffs, N. J.

Southall, B. L., et al. (2007), Marine mammal noise exposure criteria: Initial scientific recommendations, *Aquat. Mamm.*, *33*(4), 411–509.

Tolstoy, M., J. B. Diebold, S. C. Webb, D. R. Bohnenstiehl, E. Chapp, R. C. Holmes, and M. Rawson (2004), Broadband calibration of R/V *Ewing* seismic sources, *Geophys. Res. Lett.*, *31*, L14310, doi:10.1029/2004GL020234.

Tolstoy, M., J. Diebold, L. Doermann, S. Nooner, S. C. Webb, D. R. Bohnenstiehl, T. J. Crone, and R. C. Holmes (2009), Broadband calibration of the R/V *Marcus G. Langseth* four-string seismic sources, *Geochem. Geophys. Geosyst.*, *10*, Q08011, doi:10.1029/2009GC002451.

Urick, R. J. (1975), *Principles of Underwater Sound*, 384 pp., McGraw-Hill, N. Y.